IEEE Access
Multidisciplinary | Rapid Review | Open Access Journal

Received 25 September 2023, accepted 23 October 2023, date of publication 31 October 2023, date of current version 6 November 2023.

Digital Object Identifier 10.1109/ACCESS.2023.3328852

RESEARCH ARTICLE

Evolutionary Optimized 3D WiFi Antennas Manufactured via Laser Powder Bed Fusion

DOMINIK MAIR[1], (Member, IEEE), MICHAEL RENZLER[1], STANISLAV KOVAR[2], (Member, IEEE), TOMAS MARTINEK[2], TOMAS KADAVY[2], SIMON BERGMUELLER[3], ANDRADA HORN[1], JAKOB BRAUN[3], AND LUKAS KASERER[3]

[1]Department of Mechatronics, Microelectronics and Implantable Systems, Faculty of Engineering Science, Universität Innsbruck, 6020 Innsbruck, Austria
[2]Faculty of Applied Informatics, Tomas Bata University in Zlín, 76005 Zlín, Czech Republic
[3]Department of Mechatronics, Materials Science—Additive Manufacturing, Faculty of Engineering Science, Universität Innsbruck, 6020 Innsbruck, Austria

Corresponding author: Dominik Mair (dominik.mair@uibk.ac.at)

This work was supported in part by the Austrian Agency for Education and Internationalisation (OeAD) in the Framework "Scientific & Technological Cooperation (S&T Cooperation)" under Grant CZ 03/2022, in part by the European Regional Development Fund (ERDF) within the K-Regio Project "SafeAviationTyrol," in part by the Austria Wirtschaftsservice Gesellschaft (AWS) under Grant P2372773, and in part by the University of Innsbruck.

ABSTRACT The swift and automated design of antennas remains a challenging aspect in research due to the specific design needs for individual applications. Alterations in resonance frequency or boundary conditions necessitate time-consuming re-designs. Though the application of evolutionary optimization and generative methods in general to antenna design has seen success, it has been mostly restricted to two-dimensional structures. In this work, we present an approach for designing three-dimensional antennas using a genetic algorithm coupled with a region-growing algorithm - to ensure manufacturability - implemented in Matlab manufactured via laser powder bed fusion (LPBF). As a simulation tool for optimization CST is used. The antenna has been optimized in a completely automated manner and was produced using the metal 3D printing technology LPBF and aluminium based AlSi10Mg powder. The presented concept, which builds upon previous two-dimensional techniques, allows for significant flexibility in design, adapting to changing boundary conditions, and avoiding the geometric restrictions seen in prior methods. The optimized antenna has a size of 3.01 cm × 3.43 cm × 1.67 cm and was measured in an anechoic chamber. According to measurements a minimum reflection coefficient of −19.95 dB at 2.462 GHz and a bandwidth of 308.8 MHz are observed. CST simulation results predict an efficiency of 98.91 % and the maximum antenna gain is measured at 2.45 GHz to be 3.27 dBi. Simulations made with CST and Ansys HFSS and measurements are in excellent agreement with a deviation of the resonance frequency of only 0.13 %, thus further establishing genetic algorithms as a highly viable option for the design of novel antenna structures.

INDEX TERMS Antennas, genetic algorithms, laser powder bed fusion (LPBF), additive manufacturing (AM).

I. INTRODUCTION

The wish for a fast and automated design of antennas is an ongoing research topic due to the fact that each antenna has to be specifically designed for its respective application. A change in resonance frequency or the boundary condition always entails a re-design, which can be time-consuming at best and rendering an application unfeasible in the worst case. In order to automate the optimization process of antennas, evolutionary or genetic algorithms have been used successfully in the past [1], [2]. By pixelating a pre-defined area novel structures can be created, that have been shown to outperform conventionally designed topologies [3], [4].

So far these techniques have been mostly limited to planar or two-dimensional pixelated antennas. However, recent advances in additive manufacturing allow for the printing

The associate editor coordinating the review of this manuscript and approving it for publication was Ravi Kumar Gangwar.

of conductive structures for RF applications [5]. Another possibility is the usage of polymer-based filaments, and the subsequent coating of the printed structures with conductive spray [6], to use adhesive tape [7] or coating techniques like physical vapour deposition [8] or others.

Adapting automated design and optimization techniques for antennas from 2D to 3D allows for a greater flexibility in the design and adaption to changing boundary conditions. Previous studies showed the possibility of using evolutionary algorithms for electromagnetic problems in 3D, such as shielding enclosures [9], [10] and also antennas.

Smith and Baginski used thin wires as basic building blocks, whose arrangement were optimized using an evolutionary algorithm [11]. By definition, the usage of such thin wires leads to a severe restriction in possible topologies. Cook et al. presented a 3D-printed fragmented aperture antenna, where the structure consists of individual voxels [12]. The arrangement of the voxels was optimized using an evolutionary algorithm, leading to a fragmented antenna, which was printed from a polymer and plated afterward. However, no detailed measurements or discussions about the algorithm were presented. Trinh-Van et al. presented a circular polarized wideband antenna using a pixelated dielectric resonator (DR) [13]. The DR consists of discretized bars, whose heights were optimized using an evolutionary algorithm and were manufactured from subdivided milled sets of alumina ceramic that were then glued together.

These previous reports inhibit several innate problems, as the flexibility of the employed method is limited by the need for post-processing, or the topology itself is restricted by design. Therefore, the possibility of manufacturing a conducting structure without geometric restrictions directly from the optimized model would be highly advantageous. Recent advances in Additive Manufacturing (AM), particularly in Laser Powder Bed Fusion (LPBF) [14], render this novel technique a viable option for manufacturing electronics in general [15] and antennas in particular [16].

In this work, we present a method to design and optimize a Wi-Fi antenna in the 2.4 GHz band (IEEE 802.11b/g/n/ac). While our prior efforts focused on algorithms strictly constrained to two dimensions [3], the current study extends this foundation by introducing novel algorithmic improvements tailored for three-dimensional applications for antennas. These advancements not only offer a broader solution space but also better adapt to the complexities and challenges of 3D antenna design. For manufacturability, a region-growing algorithm featuring 14-connected neighborhood specifically designed for 3D voxelated antennas is presented. The optimized structures were then produced using LPBF using an AconityMIDI by Aconity3D. The manufactured antennas were measured in an anechoic chamber and the achieved results are in excellent agreement with the simulations.

This is the first report of a 3D-antenna consisting of individual voxels optimized using evolutionary algorithms and manufactured by LPBF. This technique allows for a high degree of flexibility, as a wide range of metals can be used and therefore, antennas can be specifically optimized for a variety of different applications scenarios. Furthermore, by extending the algorithm from two to three dimensions, the solution space for the generated antennas is enhanced significantly, allowing antennas to be created for severely restricted geometries.

II. METHODS

A. OPTIMIZATION METHOD

The basic implementation of the optimization scheme for the 2D-case has been described previously [3]. The distinction in this present study is that the three-dimensional antennas consist of three-dimensional building blocks, i.e. voxels, instead of pixels as described previously. This has direct consequences for the way the antenna can be manufactured, as mechanical stability has to be accounted for and floating voxels (i.e. voxels that are not connected to other voxels) have to be avoided. Therefore, a region-growing algorithm has been implemented.

The optimization scheme is implemented in Matlab using the *ga-function*. At the start of the optimization, 50 randomly filled boolean strings (or individuals) are created, which represents an initial population. 50 corresponds to the population size. With the help of a CST Matlab Interface [17] this population is then converted into a CST Studio Suite project. For CST the frequency domain solver with adaptive tetrahedral mesh was employed. CST simulates properties like antenna gain or reflection coefficient of each individual. These parameters are then handed back to our algorithm, which calculates a fitness function and afterward employs evolutionary methods (i.e. genetic operators) to create a second population, which again is simulated. The whole process is repeated in iterative manner until the desired target goal has been reached.

In the following paragraphs, a general description of the genetic algorithm and the employed methods is given, which is followed by a detailed account on the voxelation process and the region-growing algorithm.

1) GENETIC ALGORITHM

One of the most famous examples from the family of evolutionary algorithms is the Genetic Algorithm (GA), developed in the 1960s by John Holland [18]. One of the distinct features of a classical GA, is the representation of the phenotype of an individual in the form of a chromosome - a binary string - which corresponds to the genotype. The bits of this string are often called genes. A whole population is therefore represented as a set of chromosomes. A GA uses three genetic operators that work in conjunction to allow for a successful optimization scheme: selection, crossover, and mutation.

a: SELECTION

The selection process determines which individuals are used for recombination and mutation. Therefore, the individuals to be selected are called parents. This selection process is

based on their fitness function value. Typically, this is done using one of the following three methods: roulette rule, rank selection, and tournament selection. Each technique affects the speed of convergence and the quality of the final solution. Individuals with a better fitness function are more likely to be selected for reproduction and passing their genes to the next generation. However, in Matlab the genetic algorithm ga has to be provided with an objective function for minimization. The employed objective function O is the mean value over $N = 3$ frequencies 2.4, 2.45 and 2.5 GHz of the inverse reflection coefficient $S_{11}|_{\mathrm{dB}}$ which is scaled by the target $S_{11,\mathrm{Max}}|_{\mathrm{dB}} = -10\,\mathrm{dB}$ as seen in equation 1. This scaling is applied, because matlab stops optimization if the objective function reaches a value of 1.

Once the reflection coefficient for any single frequency reaches $-10\,\mathrm{dB}$, the objective function is capped at 1 for the purpose of the average calculation. This ensures a balanced optimization across all frequencies.

Matlab calculates the fitness of the results provided by the objective function by applying the rank based fitness scaling *@fitscalingrank*. The fitscalingrank function performs rank-based fitness scaling for a single objective in a genetic algorithm. It takes the values obtained from an objective function (scores) and the number of parents (nParents) as inputs. The function calculates the fitness of the scaled values based on ranks. It sorts the objective function values in ascending order and assigns scaled values to individuals based on their rank in the sorted list. Lower ranks (better objective function values) receive higher scaled values. Rank-based fitness scaling enhances the controlled adjustment of objective function values used for selecting parents in a genetic algorithm. Applying this scaling increases the selection pressure on the best individuals according to the objective function, making them more likely to be chosen as parents. This can accelerate the convergence speed of the genetic algorithm and make the search in the solution space more effective.

$$O(S) = \frac{1}{N}\sum_{i=1}^{N} \max\left(1, \left|\frac{S_{11,\mathrm{MaxdB}}}{S_{11,i}|_{\mathrm{dB}}}\right|\right) \tag{1}$$

Matlab GA includes *Stochastic Universal Sampling* [19] as a default selection method. This selection method lays out a line of length F in which each parent corresponds to a section of the line of length proportional to its scaled value as shown in Fig.1 for an example population of 6 antennas. The length is based on the calculated fitness of CST Studio Suite simulation results. The algorithm moves along the line in equal steps, and each step allocates a parent it lands on.

b: CROSSOVER

Crossover creates offsprings (i.e. children) from a combination of two different solutions (parents). Several types of crossover implementations exist, in this study *Crossover Scattered* [20] was used. Crossover Scattered creates a random binary vector R, where "1" indicates that genes are

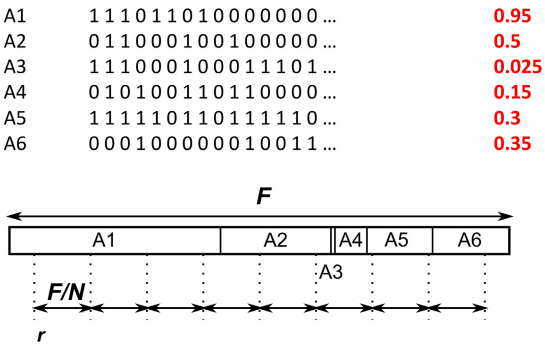

FIGURE 1. Graphical representation of stochastic universal sampling for an example population of 6 antennas.

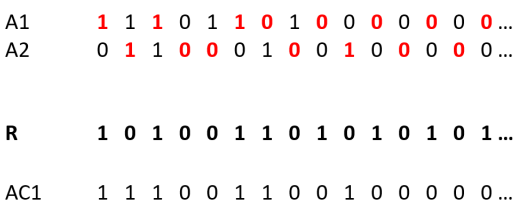

FIGURE 2. Schematic representation of recombination. Vector R selects genes from the parents A1 and A2 and a combination or "child" AC1 is formed.

selected from the first parent and "0" indicates that genes are selected from the second parent. The resulting offspring or child is therefore made up of genes from both parents. Fig.2 exemplifies this process for two parents, A1 and A2, and "their child" AC1. As a recombination rate 0.8 is chosen.

c: MUTATION

The last step in a genetic algorithm is mutation. During this process, chromosomes of individuals from the initial population are altered randomly, by inverting the binary value associated with some of the genes, i.e. switching them from "1" to "0" or vice versa as exemplarily shown in Fig.3. The mutation's primary goal is to maintain diversity within the population and prevent premature convergence. These mutated individuals are then added to the new population for the next generation. In this study the Matlab function *mutationuniform* was used, which selects a fraction of the vector entries of an individual for mutation. Each entry has a certain probability of being mutated. In the course of this study, a mutation rate of 0.01 was used. Each selected entry has then a 50% probability of being replaced by either "1" or "0" respectively.

The steps covered in this brief description represent only one variant of a GA. Its pseudo-code is shown in Algorithm 1. Over the years, a vast number of different versions of GA's emerged, many of them are specifically designed to solve distinct problems [21], [22], [23].

Limitations Regarding Chosen Parameters and Strategies: It should be emphasized that neither the selected genetic strategies nor the parameters - mutation rate, recombination rate, and population size - used in this study were subjected

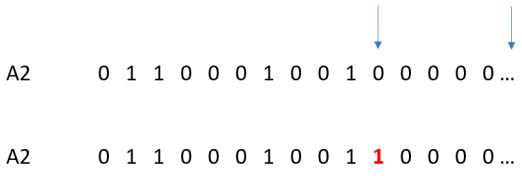

FIGURE 3. Schematic representation of mutation.

Algorithm 1 Genetic Algorithm

```
GA initialization
while Stopping criterion not met do
    for i = 1toNPwithi+ = 2 do
        Selection step
        Crossover step
        Mutation step
    end for
    record the best solution
end while
```

to a tuning analysis and, thus, may not be optimal. However, they are detailed here expressly for the sake of reproducibility. Further research is needed to assess the optimal parameters for different target function as well as antenna and voxel sizes.

2) VOXELATION

As explained above, the fragmented antenna in this study is made up of three-dimensional basic building blocks, called voxels. Initially, boundary conditions like employed materials and the maximum dimensions of an antenna $\vec{D}$ have to be set.

$$\vec{D} = \begin{bmatrix} L_{\max} \\ W_{\max} \\ H_{\max} \end{bmatrix} \tag{2}$$

This volume with dimensions $\vec{D}$ is then voxelated with small cubic elements of size $\vec{d}$:

$$\vec{d} = \begin{bmatrix} L_{\text{cub}} \\ W_{\text{cub}} \\ H_{\text{cub}} \end{bmatrix} \tag{3}$$

As a first step, l cubes are positioned in a line in the y-direction as depicted in Fig.4 with

$$l = \frac{W_{\max}}{W_{\text{cub}}} \tag{4}$$

This process is continued for more lines until a single layer with

$$m = \frac{L_{\max}}{L_{\text{cub}}} \tag{5}$$

lines is formed.

In order to avoid singularities in the optimization process like edge-to-edge contacts between neighboring voxels in a layer, every second line is shifted in the y-direction by $-W_{\text{cub}}/2$.

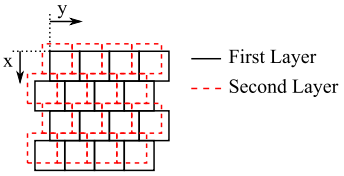

FIGURE 4. Voxelation scheme showing first and second voxelated layer.

This process is continued in the z-direction layer by layer until the cube is filled with

$$n = \frac{H_{\max}}{H_{\text{cub}}} \tag{6}$$

layers. Again, in order to avoid singularities between elements in different layers, also every second layer has to be shifted. For shifting in x-direction a value of $-L_{\text{cub}}/4$ and in y-direction a value of $-W_{\text{cub}}/4$ is chosen. It should be noted here, that the shifting value of a layer needs to be different from the shifting value for line shifts, due to the fact, that singularities could occur in the later optimization process if the shifts would be the same.

These voxels can now be turned on or off by changing their material properties to conductive or non-conductive, respectively, by the employed simulation software package CST Studio Suite. The structure of an antenna is represented as a three-dimensional boolean array R with size $l \times m \times n$ in which "1" corresponds to a conductive and a "0" corresponds to a non-conductive element. This renders an evolutionary optimization possible in the first place, as described above.

The feeding of the antenna is generated by a structure as depicted in Fig.5. It is placed in the middle of the first and second layer and guarantees, that under no circumstances a shorted port occurs. The black voxels, marked as P1 and P2, indicate the physical representation of the two port voxels, that have to be conductive. The red arrow depicts this port, as implemented in CST Studio Suite, as it originates from the right face's center of P1 to the left face's center of P2.

3) REGION-GROWING ALGORITHM

In order to be able to produce a 3D voxelated antenna with methods like LPBF some restrictions on the solution space have to be made. First, floating voxels without any connection to the port are not allowed. Second, for structural stability, the two arms extending from the port have to be connected at some point. Both constraints can be achieved by using a region-growing algorithm.

In the following text, a voxel element i, in the line j and layer k for the region-growing algorithm is defined by:

$$E(i, j, k)$$

In order to successfully implement a region-growing algorithm, the neighborhood of each individual voxel has to be defined. In general, this means that the neighbors of a voxel in the same layer k, the layer above $(k + 1)$, and

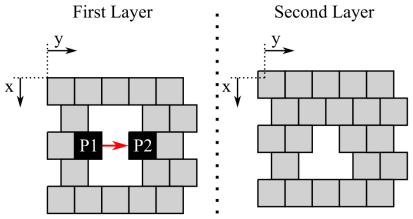

FIGURE 5. Placement of antenna feed on the bottom layer and the subsequent placement of the second layer. The red arrow indicates the feeding as designed in CST.

the layer below $(k-1)$ have to be observed. However, unlike standard structures, 3D voxelated antennas feature shifted lines and shifted layers. Thus, in this publication, we introduce a new type of connected neighborhood, termed the 14-connected neighborhood, specifically designed for this application. Therefore, the neighborhood of a voxel $E(i, j, k)$ is dependent on the exact location of this voxel. To be specific, there are six different cases of a voxel's neighborhood, as depicted in Fig.6.

In order to let the algorithm run efficiently, the indices i,j and k of voxels $E(i, j, k)$ that have to be observed in an iteration, are stored in a table T and already observed voxels in a table O. A three-dimensional array R contains all voxels connected to P1 and therefore the antenna structure.

In the first iteration, the only voxel stored within T is the port voxel P1 and R is empty. Lookup-tables are present in the code which tell the algorithm which neighbors have to be observed, based on the illustration shown in Fig.6. If a voxel V in the neighborhood is conductive, this voxel is stored into the table T and O. Voxel P1, wich has been observed in the first iteration, is deleted from T and the corresponding voxel is set to 1 in R.

Again, the voxels in the table T are reviewed, and the neighborhoods are observed, according to Fig.6. Table T is filled with the new voxels found to be conductive. However, they are only stored in T if they are not yet present in O. Voxels observed in the iteration are deleted from T and stored in R. This process is executed iteratively, until the table T is empty.

If P1 and P2 are stored in T during the initial iteration, each arm extending from a port voxel is a connected arm and no floating voxels occur in R. The region-growing algorithm is started from P1 only and it is checked if the port voxel P2 is stored in matrix R. This assures, that the ports are connected by conducting material and therefore more structural stability is achieved. If P2 is not within R, the antenna is assigned a penalty value during the calculation of the fitness function.

Using the discussed approach, antennas for the frequencies of 2.4, 2.45 and 2.5 GHz and sizes of 3.01 cm × 3.43 cm × 1.67 cm were optimized. In order to check the validity of our optimization, all results are cross-checked with Ansys HFSS. In the next paragraphs, a detailed description on the manufacturing process will be given.

4) ADDITIVE MANUFACTURING

The antennas were manufactured from the material AlSi10Mg using the additive manufacturing process LPBF. Powder from the company SLM Solution with a particle size of 20 µm to 63 µm was used. The chemical composition of the AlSi10Mg powder complies with DIN EN 1706:2013 and the powder contains between 9-11 wt.% Si, 0.20-0.45 wt.% Mg, <0.55 wt.% Fe, <0.55 wt.% Mn, <0.15 wt.% Ti, <0.10 wt.% Zn and <0.05 wt.% Cu, Ni, Pb and Sn.

A customized LPBF system AconityMIDI (Aconity3D Gmbh, Germany) equipped with a 1000 W IPG Yb:YAG laser (IPG Laser GmbH, Germany) was used for the production of specimens. Argon was used as a process gas, and the oxygen level in the building chamber was kept below 50 ppmv. A nominal layer thickness of 50 µm and a substrate plate preheating temperature of 220 °C was used. For each layer, the hatch pattern was rotated by 67°. A stripe scan strategy was used, with scan vectors in meander sequence (zigzag), and vector lengths of 5 mm. The laser power was set to 400 W, scan speed to 1350/2000 mm s^{-1} for hatches/contour, hatch distance to 150 µm and laser spot size to 90 µm. This parameter set is the standard set of processing instructions developed by Aconity3D GmbH for working with AlSi10Mg alloy on AconityMidi machines. They have been optimized by Aconity3D to enhance both the density and mechanical properties of the final product.

The antenna was built rotated by 45° around the x-axis compared to the orientation in Fig. 7. This allowed that support structures were only required on the down-facing edges of each voxel, using 0.4 mm thick wall supports. As a result, the removal of supports is minimally difficult and all side surfaces have a similar surface quality.

The resistivity of a component crafted from AlSi10Mg powder hinges on multiple factors, including the specific manufacturing process. Silbernagel et al. conducted an investigation into the electrical resistivity of LPBF produced structures [24]. This study involved the fabrication of multiple test bars, each measured five times using a micro-ohmmeter. The results determined the worst resistivity to be in mean 9.87 µΩ cm, corresponding to a conductivity of 10.1 MS m^{-1}. This conductivity value has been employed for all simulations within this publication.

Fig.7 shows a picture of one of the manufactured antennas and the corresponding simulation model.

B. ANTENNA MEASUREMENTS

Due to the differential feeding, the antenna's impedance is measured by using the differential impedance measurement technique published by Qing et al. [25]. This concept employs a VNA with at least two ports. A TOSM calibration scheme is applied to the cables connected to the VNA. The test fixture, attached to these cables, is composed of two semi-rigid coaxial cables that are soldered together at their outer shields. The ends of the semi-rigid cables not connected to the VNA are to be connected to an antenna under test. To eliminate the test fixture's unwanted phase shift

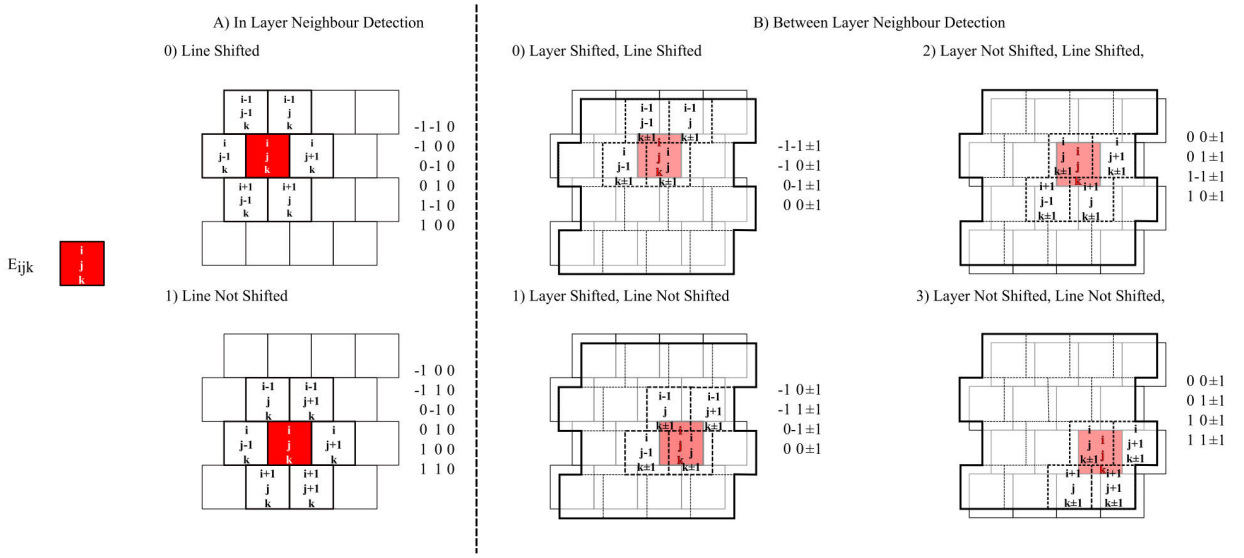

FIGURE 6. Different cases of the neighborhood of a voxel $E(i, j, k)$ marked in red. If the neighborhood in the same layer as the voxel is observed, the two cases shown in A) exist. Either the voxel is A0) positioned in a line that is shifted or it is A1) in a line that is not shifted. If the neighborhood in a layer above or below a voxel is observed the four cases in B) emerge. Either the voxel is B0) positioned in a layer and a line which are shifted, B1) positioned in a layer which is shifted but the line is not, B2) positioned in a layer which is not shifted but the line is shifted or B3) positioned in a layer and a line which are both not shifted.

and losses, a port extension technique is used. This involves measuring the shorted test fixture to shift the calibration plane. The antenna's port voxels are then attached to the inner conductors of the semi-rigid coaxial cables, and two-port scattering parameter measurements are performed. Due to the asymmetrical structure of the voxelated antenna, the following formula can be applied to calculate the antenna's input impedance Z_d from the measured scattering parameters:

$$Z_d = \frac{2\,Z_0\,(1 - S_{11}S_{22} + S_{12}S_{21} - S_{12} - S_{21})}{(1 - S_{11})(1 - S_{22}) - S_{12}S_{21}} \qquad (7)$$

In this equation, Z_0 is the characteristic impedance of the connected transmission lines. The antenna's differential impedance Z_d can then be calculated into the differential scattering parameter S_{dd11}.

During the gain measurement, coat waves can occur due to unbalanced currents resulting from the unbalanced (coaxial) to balanced (antenna) connection. These coat waves can result in pattern squints due to radiation from the cable. They can be reduced by introducing a sleeve Balun in the measurement setup. In this study, the Balun was designed for a frequency of 2.45 GHz. The outer diameter of the employed coaxial cable is 3.58 mm and the inner diameter of the employed copper pipe is 10 mm. Due to fringing fields at the end of the Balun, the produced sleeve was chosen to have a length of $0.237\lambda = 29.03$ mm [26].

The measurement procedure has already been used and tested for a variety of different application scenarios [3], [4], [27].

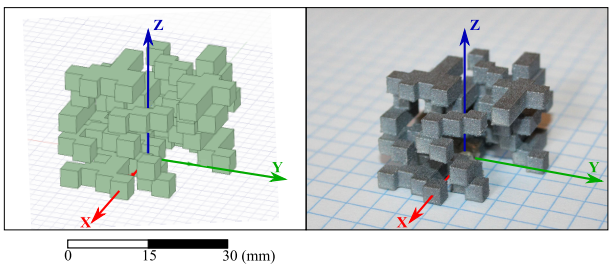

FIGURE 7. Picture of the simulated antenna (left) and the corresponding manufactured structure (right).

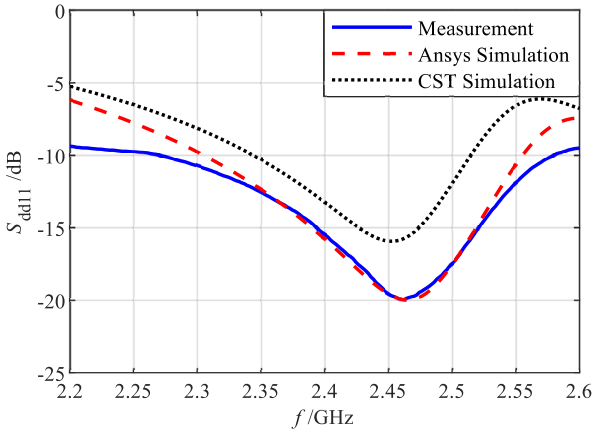

FIGURE 8. The simulated reflection coefficient S_{dd11} for Ansys HFSS (dashed red line) and CST (dotted black line) compared to measurement results (solid blue line).

III. RESULTS AND DISCUSSION

The algorithm described in II-A generated the antenna, as depicted in Fig. 7. Roughness was not taken into consideration. This assumption is justified as shown by the

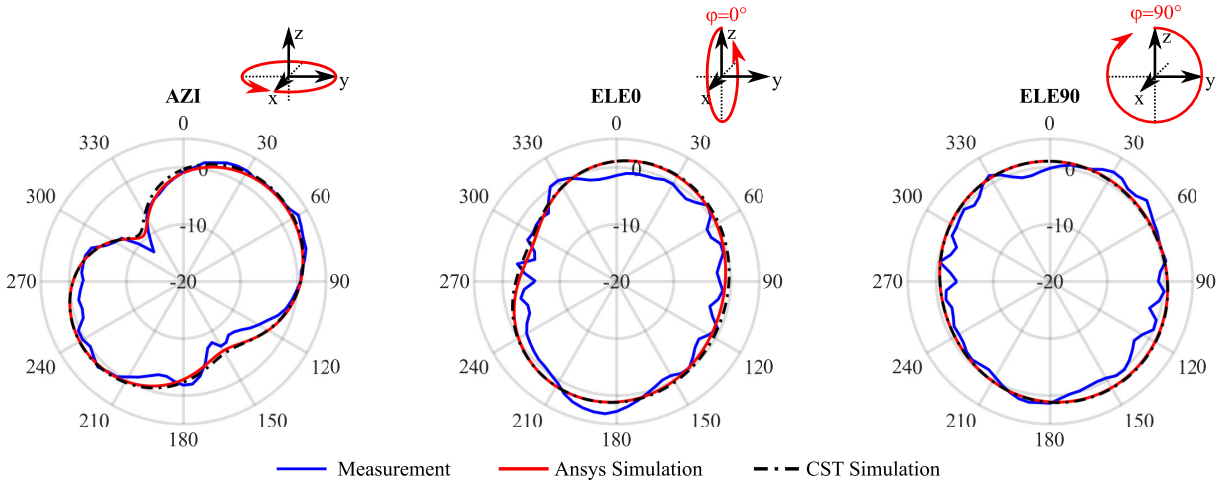

FIGURE 9. Antenna gain patterns for azimuth (AZI, $\vartheta = 90°, \varphi = 0°$ to $180°$), elevation 0 (ELE0,$\varphi = 0°, \vartheta = -180°$ to $180°$) and elevation 90 (ELE90,$\varphi = 90°, \vartheta = -180°$ to $180°$) angles. Measurements are indicated by a solid blue line, simulations performed with Ansys HFSS are drawn by a solid red line, and simulations performed with CST are indicated by a dash-dotted black line.

following results. However, as detailed in Sec. II-A4, the material features a conductivity of $\sigma = 10.1\,\mathrm{MS\,m^{-1}}$ which is why all simulations in this section are performed with this value. Although the antenna was optimized using CST and Matlab, simulations were also conducted with Ansys HFSS to validate the optimization results. Fig. 8 illustrates the measured and simulated reflection coefficient S_{dd11}.

CST predicts a resonance frequency of 2.452 GHz with a matching of −15.92 dB, and Ansys HFSS anticipates a resonance frequency of 2.465 GHz with a matching of −19.97 dB. Measurements reveal a resonance frequency of 2.462 GHz with a matching of −19.95 dB. Ansys and CST respectively predict bandwidths of 249.3 MHz and 170.8 MHz, compared to a measured bandwidth of 308.8 MHz. A summary of these results can be found in Table 1.

TABLE 1. Observed resonance frequency f_{r}, minimum reflection coefficient $\min(S_{\mathrm{dd11}})$ and bandwidth BW for simulation in Ansys HFSS and CST, and measurement.

	f_{r} (GHz)	$\min(S_{\mathrm{dd11}})$ (dB)	BW (MHz)
Ansys HFSS	2.465	-19.97	249.3
CST	2.452	-15.92	170.8
Measurement	2.462	-19.95	308.8

It can be observed that the deviation between the simulated and measured resonance frequencies is quite low, with relative deviations of 0.13 % for Ansys and 0.4 % for CST. However, CST exhibits a greater discrepancy in the magnitude of the reflection coefficient, resulting in a minimum reflection coefficient 4.03 dB higher than the measurement, whereas Ansys more closely aligns with the observed values. Deviations between simulation and measurement can be attributed to factors such as non-ideal test fixtures and inaccuracies in the manufacturing of the three-dimensional antenna as well as simulation errors. In order to account for naturally occurring deviations in simulation results using different simulation tools, we opted for a comparison between measurements and simulations obtained via Ansys HFSS and CST.

Nevertheless, both Ansys and CST predict that the antenna will be matched across the full WiFi 2.4 GHz band.

While the reflection coefficient provides valuable insights into the impedance matching of the antenna, it is not solely sufficient for a comprehensive antenna design; the observation and optimization of the antenna gain are equally crucial to ensure robust performance and efficiency.

Simulations were conducted to assess both the antenna's efficiency and the gain patterns, the latter of which were also measured. The efficiency was computed using both Ansys and CST, yielding results of 99.35 % and 98.91 %, respectively. The antenna's gain patterns for the coordinate system despicted in Fig. 7, are illustrated in Fig. 9. These patterns include the azimuth (in spherical coordinates $\vartheta = 90°, \varphi = 0°$ to $180°$), elevation at 0 degrees (with coordinates $\varphi = 0°, \vartheta = -180°$ to $180°$), and elevation at 90 degrees (with coordinates $\varphi = 90°, \vartheta = -180°$ to $180°$).

The pronounced similarity between the simulations and measurements results in a low mean absolute error (MAE). Specifically, the MAE between Ansys and the measurements is 0.93 dB for azimuth, 1.27 dB for elevation at 0°, and 1.13 dB for elevation at 90°. Similarly, the MAE between CST and the measurements is 1.02 dB for azimuth, 1.44 dB for elevation at 0°, and 1.16 dB for elevation at 90°. It is noteworthy that both CST and Ansys predict gain patterns that are closely aligned. The maximum gains determined by Ansys and CST are 2.18 dBi and 2.48 dBi respectively, compared to a measured value of 3.27 dBi. A summary of these results, including the MAE and maximum gains, can be found in Table 2. The discrepancies between the simulation and measurement results can be attributed to factors such as a non-ideal sleeve Balun, leading to imperfect filtering of

common mode waves manifesting as wobbles in the pattern, and imperfections in the manufacturing of the antenna.

TABLE 2. Summary of gain pattern data for azimuth (AZI, $\vartheta = 90°, \varphi = 0°$ to $180°$), elevation 0 (ELE0,$\varphi = 0°, \vartheta = -180°$ to $180°$) and elevation 90 (ELE90,$\varphi = 90°, \vartheta = -180°$ to $180°$) angles.

	AZI	ELE0	ELE90
Ansys HFSS			
Efficiency		99.35 %	
MAE	0.93 dB	1.27 dB	1.13 dB
Max Gain	2.19 dBi	1.39 dBi	1.50 dBi
CST			
Efficiency		98.91 %	
MAE	1.02 dB	1.44 dB	1.16 dB
Max Gain	2.48 dBi	1.46 dBi	1.61 dBi
Measurement			
Max Gain	3.24 dB	3.27 dB	2.15 dB

IV. CONCLUSION

This work is the first detailed study of using evolutionary algorithms for the optimization of three-dimensional antennas manufacturable by LPBF. A region-growing algorithm was implemented, to avoid floating voxels and mechanical stability to ensure manufacturability. The optimized structure with a size of 3.01 cm × 3.43 cm × 1.67 cm was manufactured from powder of the aluminium alloy AlSi10Mg by LPBF and measured in an anechoic chamber.

According to measurements the minimum reflection coefficient is −19.95 dB at a frequency of 2.462 GHz and the gain is measured to be 3.27 dBi at 2.45 GHz with a simulated efficiency of 99.35 % according to Ansys HFSS and 98.91 % according to CST. While this publication should serve as a first study on the possibility of using additive manufacturing for the production of complex, three-dimensional radio-frequency devices, the excellent agreement between simulated data and experiment, paves the way for further studies. It is also noteworthy, that this study shows high efficiencies for three-dimensional antennas produced with AlSi10Mg. According to Silbernagel et al. [24] heat treatment of this material reduces its electrical resistivity. Due to the already high achieved efficiencies, it is assumed, that further heat treatment does only result in a minor performance gain for in this study observed frequencies in the range of 2.45 GHz. However, this should be examined in the future for different antenna- and voxel- sizes for different frequencies.

Future work will concentrate on characterizing the electrical material properties of novel materials, such as permittivity, permeability, and resistivity, which have a significant influence on an antenna's performance. Comparative studies using different powders will be conducted to assess their potential for RF applications.

Identifying the optimal values for evolutionary optimization parameters like mutation and recombination rates as well as identifying optimal strategies requires a thorough investigation in the future. In this work the antenna was optimized only regarind a low reflection coefficient. However, it should be possible to optimize for gain or to generate specific radiation pattern shapes. This will be observed in further studies. Additionally, the constraints of the technique presented here will be explored through the optimization and fabrication of electrically small antennas embedded in substrates, suitable for applications in confined spaces and for antennas in the SHF range and beyond.

However, high-frequency applications present unique challenges, as higher frequencies inevitably lead to smaller structures. Consequently, the surface roughness resulting from additive manufacturing, due to the staircase effect, powder adhesion, and the melting process, can introduce additional losses that potentially degrade the antenna's operational efficiency [28]. In our current work, which focuses on the 2.4 GHz band, surface roughness is not observed as a limiting factor for the antenna's performance. However, applying the presented method to 5G applications and beyond requires a more in-depth exploration of the manufacturing process. This involves optimizing printing parameters to achieve smoother surfaces and utilizing post-processing techniques [29], [30]. Furthermore, the manufacture of increasingly small voxels might become impractical. Therefore, employing algorithms to smooth the antenna's surface during the optimization process, resulting in organic surfaces rather than voxelated ones, could enhance manufacturability. Additionally, the choice of material also affects the surface finish and losses due to surface resistance. Materials such as CoCr and Ti6Al4V have been shown to exhibit lower losses at microwave frequencies compared to aluminum [30].

An intriguing avenue for exploration involves evaluating antennas that are produced only in the outer layer of the three-dimensional structure. As current primarily flows up to the skin depth, this approach could reduce the power uptake, powder, and time required for production as well as the weight of the antennas. Furthermore, mechanical stability is going to be included in the optimization process. Such considerations may prove valuable in contexts such as aerospace applications.

REFERENCES

[1] J. Dong, Q. Li, and L. Deng, "Design of fragment-type antenna structure using an improved BPSO," *IEEE Trans. Antennas Propag.*, vol. 66, no. 2, pp. 564–571, Feb. 2018.

[2] X. Jia and G. Lu, "A hybrid Taguchi binary particle swarm optimization for antenna designs," *IEEE Antennas Wireless Propag. Lett.*, vol. 18, no. 8, pp. 1581–1585, Aug. 2019.

[3] D. Mair, M. Renzler, A. Pfeifhofer, and T. Ußmüller, "Evolutionary optimization of asymmetrical pixelated antennas employing shifted cross shaped elements for UHF RFID," *Electronics*, vol. 9, no. 11, p. 1856, Nov. 2020.

[4] D. Mair, M. Fischer, J. Konzilia, M. Renzler, and T. Ussmueller, "Evolutionary optimization of antennas for structural health monitoring," *IEEE Access*, vol. 11, pp. 4905–4913, 2023.

[5] T. D. Ngo, A. Kashani, G. Imbalzano, K. T. Q. Nguyen, and D. Hui, "Additive manufacturing (3D printing): A review of materials, methods, applications and challenges," *Composites B, Eng.*, vol. 143, pp. 172–196, Jun. 2018.

[6] J. Tak, D. Kang, and J. Choi, "A lightweight waveguide horn antenna made via 3D printing and conductive spray coating," *Microw. Opt. Technol. Lett.*, vol. 59, no. 3, pp. 727–729, Jan. 2017.

[7] M. Li and C. Yang, "Conductive adhesives as the ultralow cost RFID tag antenna material," in *Current Trends and Challenges in RFID*. Orlando, FL, USA: InTech, Jul. 2011.

[8] Ł. Januszkiewicz, S. Hausman, I. Nowak, and I. Krucińska, "Textile vee antena made with PVD process," *Int. J. Appl. Electromagn. Mech.*, vol. 46, no. 2, pp. 361–365, Jul. 2014.
[9] S. Kovar, J. Valouch, T. Kadavy, M. Pospisilik, and M. Adamek, "Enclosure shielding effectiveness calculation using SHADE algorithm," in *Proc. 19th Int. Sci. Conf. Electr. Power Eng. (EPE)*, May 2018, pp. 1–9.
[10] T. Kadavy, S. Kovar, R. Senkerik, and M. Pluhacek, "On the design of a front-face grid for shielding enclosure using evolutionary computations," in *Proc. Photon. Electromagn. Res. Symp. Fall (PIERS Fall)*, Dec. 2019, pp. 443–450.
[11] J. S. Smith and M. E. Baginski, "Thin-wire antenna design using a novel branching scheme and genetic algorithm optimization," *IEEE Trans. Antennas Propag.*, vol. 67, no. 5, pp. 2934–2941, May 2019.
[12] K. R. Cook, D. K. Richardson, J. K. Htay, J. B. Dee, and C. T. Howard, "A 3D printed fragmented aperture antenna," in *Proc. IEEE Int. Symp. Antennas Propag. USNC-URSI Radio Sci. Meeting*, Jul. 2019, pp. 1–9.
[13] S. Trinh-Van, Y. Yang, K.-Y. Lee, and K. Hwang, "A wideband circularly polarized pixelated dielectric resonator antenna," *Sensors*, vol. 16, no. 9, p. 1349, Aug. 2016.
[14] P. Mair, J. Braun, L. Kaserer, L. March, D. Schimbäck, I. Letofsky-Papst, and G. Leichtfried, "Unique microstructure evolution of a novel Ti-modified Al-Cu alloy processed using laser powder bed fusion," *Mater. Today Commun.*, vol. 31, Jun. 2022, Art. no. 103353.
[15] S. Hou, S. Qi, D. A. Hutt, J. R. Tyrer, M. Mu, and Z. Zhou, "Three dimensional printed electronic devices realised by selective laser melting of copper/high-density-polyethylene powder mixtures," *J. Mater. Process. Technol.*, vol. 254, pp. 310–324, Apr. 2018.
[16] Z. Wang, B. Zhang, and K. Huang, "A metallic 3D printed K-band quasi-pyramidal-horn antenna array," *Int. J. RF Microw. Comput.-Aided Eng.*, vol. 30, no. 7, Mar. 2020, Art. no. e22217.
[17] HGiddens. (Nov. 1, 2023). *Hgiddenss/cst_app*. Github. [Online]. Available: https://github.com/hgiddenss/CST_App
[18] J. H. Holland, "Genetic algorithms," *Sci. Amer.*, vol. 267, no. 1, pp. 66–73, 1992.
[19] T. Pencheva, K. Atanassov, and A. Shannon, "Modelling of a stochastic universal sampling selection operator in genetic algorithms using generalized nets," in *Proc. 10th Int. Workshop Generalized Nets*, Sofia, 2009, pp. 1–7.
[20] C. S. Ooi, M. H. Lim, and M. S. Leong, "Self-tune linear adaptive-genetic algorithm for feature selection," *IEEE Access*, vol. 7, pp. 138211–138232, 2019.
[21] M. Squires, X. Tao, S. Elangovan, R. Gururajan, X. Zhou, and U. R. Acharya, "A novel genetic algorithm based system for the scheduling of medical treatments," *Exp. Syst. Appl.*, vol. 195, Jun. 2022, Art. no. 116464.
[22] X. Zhang and C. Yang, "Application of multipopulation genetic algorithm in industrial special clothing design," *Wireless Commun. Mobile Comput.*, vol. 2022, pp. 1–9, Jul. 2022.
[23] G. Marasco, G. Piana, B. Chiaia, and G. Ventura, "Genetic algorithm supported by influence lines and a neural network for bridge health monitoring," *J. Structural Eng.*, vol. 148, no. 9, Sep. 2022, Art. no. 04022123.
[24] C. Silbernagel, I. Ashcroft, P. Dickens, and M. Galea, "Electrical resistivity of additively manufactured AlSi10Mg for use in electric motors," *Additive Manuf.*, vol. 21, pp. 395–403, May 2018. [Online]. Available: https://www.sciencedirect.com/science/article/pii/S2214860418300769
[25] X. Qing, C. Khan Goh, and Z. Ning Chen, "Impedance characterization of RFID tag antennas and application in tag co-design," *IEEE Trans. Microw. Theory Techn.*, vol. 57, no. 5, pp. 1268–1274, May 2009.
[26] S. A. Saario, J. W. Lu, and D. V. Thiel, "Full-wave analysis of choking characteristics of sleeve Balun on coaxial cables," *Electron. Lett.*, vol. 38, no. 7, pp. 304–305, Mar. 2002.
[27] D. Mair, M. Unterladstaetter, M. Renzler, and T. Ussmueller, "Evolutionary optimized pixelated antennas for 5G IoT communication," in *Proc. 52nd Eur. Microw. Conf. (EuMC)*, Sep. 2022, pp. 548–551.
[28] S. Baua, G. Gampala, and C. J. Reddy, "Effect of surface roughness on antenna array for automotive radar applications," in *Proc. Int. Appl. Comput. Electromagn. Soc. Symp. (ACES)*, Aug. 2021, pp. 1–3.
[29] T. Yang, T. Liu, W. Liao, E. MacDonald, H. Wei, X. Chen, and L. Jiang, "The influence of process parameters on vertical surface roughness of the AlSi10Mg parts fabricated by selective laser melting," *J. Mater. Process. Technol.*, vol. 266, pp. 26–36, Apr. 2019.
[30] N. Clark, S. Hefford, and A. Porch, "Effect of build orientation and surface finish on surface resistance in microwave components produced by selective laser melting," in *Proc. 47th Eur. Microw. Conf. (EuMC)*, Oct. 2017, pp. 508–511.

DOMINIK MAIR (Member, IEEE) received the degree in mechatronics from the University of Innsbruck, in 2012, the master's degree, in 2017, and the Ph.D. degree in technical science, in 2021. His Ph.D. thesis "Optimization of Wireless Communication Systems for the Internet of Things," earned him among others the Award of Excellence from the Austrian Government. He is currently a Senior Lecturer with the University of Innsbruck. His research interests include wireless passive systems, innovative antenna designs, additive manufacturing for antennas, antennas in challenging environments, and optimizing metamaterials.

MICHAEL RENZLER received the bachelor's degree in physics from Leopold-Franzens-University, Innsbruck, in 2010, the joint master's degree in physics from the University of Innsbruck, in 2013, and the Ph.D. degree from the Nano-Bio-Physics Group, Institute of Ion Physics and Applied Physics, in September 2016. His Ph.D. dissertation "Electron Interactions With (Doped) Helium Nanodroplets." In October 2016, he joined the Institute of Mechatronics, where he currently holds a position as a Senior Scientist. His research interests include the optimization of antennas and metamaterials and novel manufacturing methods for electromagnetic structures.

STANISLAV KOVAR (Member, IEEE) received the degree in security technology, systems, and management and the Ph.D. degree from Tomas Bata University (TBU) in Zlín, in 2014 and 2020, respectively. His Ph.D. studies defended his dissertation on "Immunity of Camera Systems Against Electromagnetic Interference." He is currently with the Department of Security Engineering, TBU in Zlín, as an Academic. He deals with electromagnetic compatibility and security technologies in his scientific research, publishing, and pedagogical activities.

TOMAS MARTINEK received the Ph.D. degree from the Faculty of Applied Informatics, Tomas Bata University (TBU) in Zlín, in September 2019. His Ph.D. dissertation "Diagnostic Methods for Percolation Threshold Determination of Ultra-Thin Tungsten Layers." He has been with the CEBIA-Tech Research Center as a Junior Researcher, since 2014. He joined the Department of Electronics and Measurements, TBU in Zlín, in 2019, as an Academician Senior Lecturer. His research interests include material properties, with an emphasis on novel materials and nanomaterials and microscopical methods, including scanning probe microscopy and electron microscopy.

TOMAS KADAVY received the M.Sc. degree in information technologies from the Faculty of Applied Informatics, Tomas Bata University (TBU) in Zlín, in 2016, where he is currently pursuing the Ph.D. degree. Since 2017, he has been a part of the AI Laboratory Team, Department of Informatics and Artificial Intelligence, TBU in Zlín. His research interests include swarm intelligence, modern swarm algorithms and their application, and evolutionary algorithms.

SIMON BERGMUELLER received the degree in mechanical engineering and the master's degree in mechatronics from the University of Innsbruck, in 2018. In the Ph.D. degree, he focuses on process optimization, application, and material development for LPBF. He is currently a Research Engineer in materials science specializing in system-based process optimization in the laser powder bed fusion process with the Materials Science—Additive Manufacturing Group, Institute of Mechatronics, University of Innsbruck.

ANDRADA HORN received the bachelor's degree in renewable energy technology from the University of Applied Sciences Weihenstephan-Triesdorf and the master's degree in environmental, process and energy engineering from the Management Center Innsbruck, in 2017. Since 2022, she has been a Technician with the University of Innsbruck, where she is involved in multiple projects focused on power electronics and electromagnetics.

JAKOB BRAUN received the bachelor's and master's degrees in materials science and engineering from Friedrich-Alexander-Universität Erlangen-Nürnberg. He is currently pursuing the Ph.D. degree in laser powder bed fusion with Leopold-Franzens-University, Innsbruck. After the master's thesis in the field of selective electron beam melting, he continued to work in the field of additive manufacturing by completing the Ph.D. studies. He is currently a senior scientist in Innsbruck, with a research focuses on alloy and process adaptation for hard-to-process alloys in LPBF.

LUKAS KASERER received the Ph.D. degree, in 2021. He has been researching the additive manufacturing process laser powder bed fusion (LPBF) of high-strength materials, since joining the Materials Science Group, University of Innsbruck, in 2016. His Ph.D. thesis ''Laser Powder Bed Fusion of the Refractory Metal Molybdenum.'' He also holds a postdoctoral research position with the University of Innsbruck, where he focuses on expanding the understanding of the unique solidification and shaping mechanisms in LPBF and tries to utilize them by developing adapted materials and process control strategies. He is currently a graduate physicist and a sports scientist.